Modular Aneutronic Fusion Engine

Gary Pajer*, Yosef Razin† and Michael Paluszek‡
Princeton Satellite Systems
6 Market Street, Suite 926, Plainsboro, NJ 08536, USA

A. H. Glasser§
Department of Aeronoautics and Astronautics, University of Washington
Seattle, WA 98195, USA

Samuel Cohen¶
Princeton Plasma Physics Laboratory
Princeton, NJ 08544 USA

ABSTRACT

NASA's JUNO mission will arrive at Jupiter in July 2016, after nearly five years in space. Since operational costs tend to rise with mission time, minimizing such times becomes a top priority. We present the conceptual design for a 10 MW aneutronic fusion engine with high exhaust velocities that would reduce transit time for a Jupiter mission to eighteen months and enable more challenging exploration missions in the solar system and beyond.

1. INTRODUCTION

Future space programs, including unmanned deep-space and manned missions to the planets, will require high power sources and high exhaust-velocity (u_e) engines. Reducing the transit time by raising u_e is desirable to reduce mission cost. Additionally for manned missions, large u_e will reduce astronaut exposure to cosmic radiation and low gravity. Manned missions also require an abort option in case of an accident or health emergency, which necessitates a high exhaust velocity/high thrust propulsion system. The exact engine specifications, particularly power and specific impulse I_{SP}, will vary for each mission. In this paper we describe a rocket engine of moderate power (10 MW), whose specific impulse would be 10^4 s or higher. Thrust can be augmented by the use of multiple engines or the injection of additional propellant. An engine and mission employing the latter scheme is described herein.

Table 1 on the following page compares various engine options, some conceptual, with exhaust velocities exceeding those attained by chemical rocket engines. The mass ratios are calculated using the rocket equation, where m_i is the initial mass, m_f is the final mass, and Δu is the total mission velocity change. The Δu used as an example in this table is that for a hypothetical voyage to Jupiter, similar to the Jupiter Icy Moon Mission (JIMO). The electric propulsion options, which accelerate ions using electric fields with or without magnetic fields, require a separate power source and therefore the mass ratios given are underestimates. One electric propulsion system, the Dual-Stage 4-Grid system, shows promise, and analysis suggests performance similar to the fusion engine described here [1]. The numbers for nuclear fusion engines are based on the direct use of fusion products as propellant, and an efficiency of 50%. This provides an unrealistic lower limit on m_i/m_f because it supplies a low thrust, on the order of 100 mN, impractical for most missions. The fusion engine described below uses thrust augmentation by the introduction of additional propellant: m_i/m_f is increased to 1.9 and the thrust to 30 N.

For unmanned missions, high Δu reduces transit time thus dramatically reducing mission costs. For example, the operational costs of Cassini are $50M USD per year. The nominal six-year transit time for JIMO would cost $300M USD. The Δu in the table is for the mission with an eighteen month transit time between Earth and Jupiter. Such a short transit time could save $225M USD, practically paying the development cost for the engine. As the table shows, only fusion engines can deliver reasonable mass fractions.

2. MODULAR FUSION ENGINE

2.1 Aneutronic Fusion Reactions

Completely aneutronic or low-neutron-production reactions are attractive for space propulsion because they reduce the required shielding and therefore reduce engine

*email address: gpajer@psatellite.com
†yrazin@psatellite.com
‡map@psatellite.com
§ahg5@u.washington.edu
¶scohen@pppl.gov

size, mass, cost, and maintenance as well. Additionally, they reduce the fraction of power not amenable to propulsion and the need to breed tritium.

The p–^{11}B aneutronic reaction, though it produces the fewest neutrons of any fusion fuel mix and the fuel is abundant, is not considered here because there is strong uncertainty whether net power could be produced and because stronger magnetic fields and higher plasma temperatures would be required.

Table 1. Comparison of propulsion technologies for a 131 km/s mission Δu. Note that the values for nuclear fusion are limiting values based on the direct use of reaction products as propellant, though this is not considered for the mission described herein. For the four electric propulsion options, the energy source, and hence the fuel, is not specified as it is external to the propulsion system. There are two entries for ion thrusters, one is a typical three-grid system, the second is the Dual-Stage 4-Grid system [1]. (See the discussion in the text.)

Type	Fuel	Propellant	u_e (km/s)	$\Delta u/u_e$	m_i/m_f
Chemical (RL-10)	LOx LH_2	H_2O	4.6	2.9×10^{4}	∞
Fusion	D–T	^{4}He	1.3×10^{4}	1.0×10^{-2}	1.01
Fusion	D–^{3}He	^{4}He+ p	2.5×10^{4}	5.3×10^{-3}	1.01
Fusion	p–^{11}B	^{4}He	1.2×10^{4}	1.1×10^{-2}	1.01
Fission	U, Pu	H_2	7.0	19	1.4×10^{8}
Nuclear Lightbulb	^{233}U	H_2	18	7.2	1.4×10^{3}
Ion (typ)		Xe	30	0.23	1.3
Ion (DS4G)		Xe	140	0.95	2.6
Hall		Ar	20	6.6	710
MPD		Li	62	2.2	8.9

We focus on the D–^{3}He plasma (deuterium–helium-3) which admits both D–^{3}He and D–D reactions.

$$\mathrm{D} + {}^3\mathrm{He} \rightarrow {}^4\mathrm{He}\ (3.6\ \mathrm{MeV}) + \mathrm{p}\ (14.7\ \mathrm{MeV}) \quad (1)$$

$$\mathrm{D} + \mathrm{D} \rightarrow \mathrm{T}\ (1.01\ \mathrm{MeV}) + \mathrm{H}\ (3.02\ \mathrm{MeV}) \quad (2)$$

$$\mathrm{D} + \mathrm{D} \rightarrow {}^3\mathrm{He}\ (0.82\ \mathrm{MeV}) + \mathrm{n}\ (2.45\ \mathrm{MeV}) \quad (3)$$

where the values in parenthesis are the energy of that particular fusion product. In our engine design the primary energy source is the D–^{3}He reaction. It provides a higher power density than the D–D reactions, and both reaction products are charged. The two D–D reactions produce $1/3$ of their power as neutrons ($f_P = 0.33$) from which it is difficult to extract useful thrust. If the tritium (T) fusion products of equation (2) also fuse within the plasma, considerably higher fractions of power would be in the undesired neutron channel. To reduce this problem two routes have been proposed. The simplest way is to reduce the D fraction in the thermal plasma from the 50%, suggested by simple stoichiometry, to 10%; this could reduce f_P to 0.07, though it would also reduce the power density if the magnetic field is held constant. Others [2, 3] have proposed an f_P-reducing method named T-suppressed D–D fusion (or He-catalyzed D–D) in which the tritium is rapidly removed from the plasma before it can fuse. The tritium is stored, naturally transmutes to ^{3}He, and is then injected into the plasma as fuel. By this circuitous route, f_P as low as 5% should be achievable. Such a cycle only makes sense for mission durations considerably longer than the half-life of tritium, 12.3 years. Our RF-plasma-heating method, to be described later, would reduce f_P to less than 0.005, by tailoring the ion energy distributions. In section 2.5 we comment on the availability of ^{3}He, a rare isotope.

2.2 Fusion Reactor Background

Many magnetic-confinement fusion reactor concepts have been proposed for rocket engines. These include:

1. Levitated dipole [4, 5]
2. Gas dynamic mirror [6]
3. Spherical tokamak with poloidal divertor [7, 8]
4. Magnetic Target Fusion with Plasma Beams [9]
5. Pulsed high density fusion rocket [10]
6. Magnetic Target Fusion with Liner [10]
7. Spherical tokamak with ripple effects for power extraction [11]
8. Beam-Heated FRC [12, 13]
9. RF-Heated FRC [14]

An important figure-of-merit for fusion reactors is β, the ratio of the plasma pressure to the magnetic energy density. Higher β means that for a given magnetic field, a greater plasma pressure is possible. Of all candidate fusion reactors, FRCs have the highest β [15]. β is close to unity in FRCs, but only 0.05 in tokamaks. Accordingly, FRC magnets would be less massive than those for a tokamak of comparable power. High β is essential for burning aneutronic fuels because they require higher ion energies to achieve the same fusion reactivity as D–T. The FRC plasma-confinement device has other attractive features, notably, a linear magnet geometry [15] and a natural divertor. These provide a magnetic nozzle for control of plasma exhaust and plume angle. The FRC is unique among quasi-toroidal closed-field-line magnetic confinement devices in that it is simply connected and has zero toroidal magnetic field, no internal conductors, and a line of zero magnetic field strength within the plasma, encircling its major axis. The null line of magnetic field is called the O-point line or the magnetic axis. The O-point line is essential for our method of RF heating.

The engine design we propose differs from [12] primarily in the heating method and size. That selected in [14] is called even-parity rotating magnetic fields [16] (RMF$_e$). Energy confinement with that method has been shown to be poor, resulting in a need for larger FRCs. Large FRCs, where the plasma radius is more than 10 or 20 times the ion Larmor radius, are prone to MHD instabilities. The RF method we select, odd-parity RMF, RMF$_o$, is predicted to promote better energy confinement, hence allow smaller, more stable engines. Ion heating by RMF$_o$ is highest near the O-point null line, *i.e.*, near the center of the plasma, on

its magnetic axis. A sketch of a 10 MW reactor is shown in Figure 1.

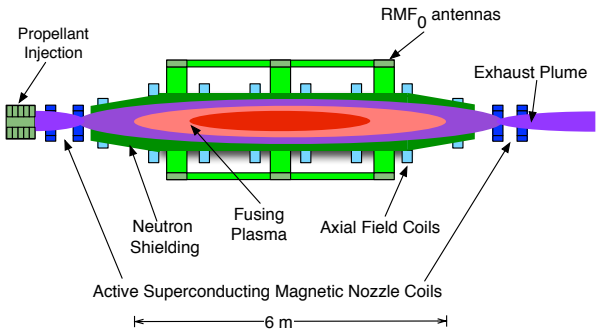

Figure 1. 10 MW reactor diagram

Many physics challenges remain before the RMF$_o$/FRC can be developed into a practical rocket engine. The primary ones are achieving adequate energy confinement, operating with excellent stability, particularly against the internal tilt mode, finding methods to sustain the plasma configuration and to heat the ions to fusion-relevant temperatures, and controlling the I_{SP} and mass flow of the propellant. Excellent progress has occurred in the first three areas. In 2010, TriAlpha Energy Corp reported near classical energy confinement time in their FRC [17]. (The "classical" value for confinement time is based on Coulomb-collision-driven diffusion. The confinement time of a real plasma is less, sometimes dramatically less, than the classical limit [18].) Our engine needs energy confinement only $1/5$ as large as the classical limit, though at considerably higher plasma temperature. In 2007, an RMF$_o$-heated FRC [19] achieved stable plasma durations 3000 times longer than predicted by MHD theory [20]. Finally, theoretical studies [21, 22, 23] indicate that RMF$_o$ will be able to heat plasma electrons and ions to fusion relevant temperatures. These are promising starts, but much research is needed at higher plasma temperature and density and with burning, *i.e.*, fusing, plasmas.

Table 2. D–^{3}He reactor [24]

Parameter	Value
Fusion power	10 MW
Neutron power	50 kW
Density electron	6×10^{20}/m^3
Temperature electron	40 keV
Avg. Energy ^{3}He	200 keV
Temperature Deuterium	100 keV
Power RMF	2 MW
Power bremsstrahlung	1.3 MW
Power synchrotron	5.4 MW
Axial magnetic field	74 kG
RMF$_o$ magnetic field	150 G

Based on the $1/5$-classical-confinement assumption, an operating point for a 10 MW RF-heated FRC rocket engine (Table 2) can be selected; a plasma radius of 25 cm is adequate for confining the high energy plasma needed to produce 10 MW of fusion power. Serendipitously, this radius matches criteria set by the RMF$_o$ heating method. The plasma temperatures listed are approximations for the full non-Maxwellian particle distributions generated and sustained by the RMF$_o$. Modest changes in parameters could increase the fusion power to 20 MW.

2.3 *The RMF$_o$ Method*

For an FRC reactor to burn its D–^{3}He fuel mix, the plasma ions must be heated to over 50 keV. If energetic neutral-beam injection were used for heating, the plasma would have to be very large, over 4 m in diameter, in order to absorb the energy of the neutral beams. Such a large reactor would produce large amounts of power, near 1 GW. In RF heating, on the other hand, power can be absorbed over shorter distances. RF heating allows the size of the reactor to be reduced by about a factor of 100 in volume and 10 in radius, to 0.5 m in diameter. A smaller volume translates to a proportionally lower power, near 10 MW, suitable for a module-based propulsion system. One characteristic of the RMF$_o$ RF method — due to a constraint set by the RMF-generated current and the FRC's magnetic field strength — is that the required RMF$_o$ frequency, ω_{RMF}, decreases as the product of plasma density times the square of the plasma radius. In contrast, the maximum ion energy is proportional to ω_{RMF}. Thus, too large or dense an FRC is not well heated. An optimum FRC for RMF$_o$ heating of ions to 100 keV and above has a radius in the range 20–30 cm. This, naturally, places a lower limit on the confinement time required, no worse than five times larger than the classical value, as noted earlier.

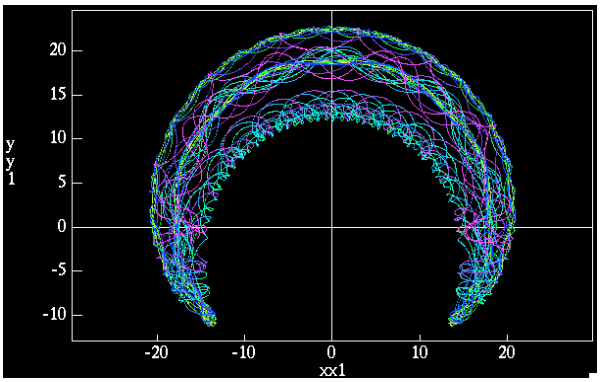

Figure 2. D$^+$ trajectory viewed in the rotating frame. The cyclotron segments of the orbit form the boundary of the crescent. The betatron segments fill the crescent closer to the O-point line, 17.7. This spatial distillation of orbit types will reduce the impact frequency of the fast betatron segments with the slower cyclotron segments.

The unique feature of the RMF$_o$ method is that it generates a time-varying azimuthal electric field near the O-point null line. This periodically accelerates and decelerates ions [21]. Choosing the RMF$_o$ frequency and amplitude properly allows ions to be pumped up, repeatedly, to an energy near the peak in the D–^{3}He fusion cross section and then returned to the bulk temperature. This is a conservative process and satisfies the recirculating energy criterion derived by Rider [25] to sustain, against collisions, a non-

Maxwellian distribution that increases the fusion rate. This situation is not possible in a plasma heated by neutral-beam injection for which there is no *handle* to repeatedly return the scattered beam ions to the desired distribution. Moreover in a D–^{3}He plasma, the trajectories of ions accelerated by RMF$_o$ are predicted to form two beams close to the FRC's O-point null line. Figure 2 shows one ion trajectory in the plane defined by the O-point null. The trajectory is viewed in the frame-of-reference rotating with the RMF. A crescent shape is clear, showing time-averaged rotational speed of the ions equal to that of the RMF$_o$. The high energy segments of the trajectory, called betatron orbits, fill the interior of the crescent while the cooler cyclotron segments of the orbits outline its edge [26].

How this situation leads to the reduction of f_p is now described. Helium-3 ions form one beam while deuterium ions constitute the other co-propagating beam. The betatron deuterium ions have half the peak energy of the ^{3}He ions, causing non-zero relative velocity between the two beams. The transverse temperature of each beam is considerably lower than the beam's peak energy, hence deuterium ions collide with each other at a far lower center-of-mass energy than with ^{3}He; accordingly, the D–D neutron production rate falls. The energy-dependent fusion rates, see Figure 3 can be used to show the basic effect of the higher energy of the ^{3}He beam. If the bulk plasma has an average energy of 70 keV and the RMF pumps the ^{3}He up by 100 keV (see line a in Figure 3) it will pump the deuterium up by only 50 keV (line b in Figure 3), increasing the former's fusion rate by a factor of 30 but the latter's only by 3. The three effects just described, low transverse beam temperature, centrally peaked betatron orbits, and higher ^{3}He energy, combine to decrease f_p to below 0.005 for an RMF$_o$-heated D–^{3}He fueled FRC.

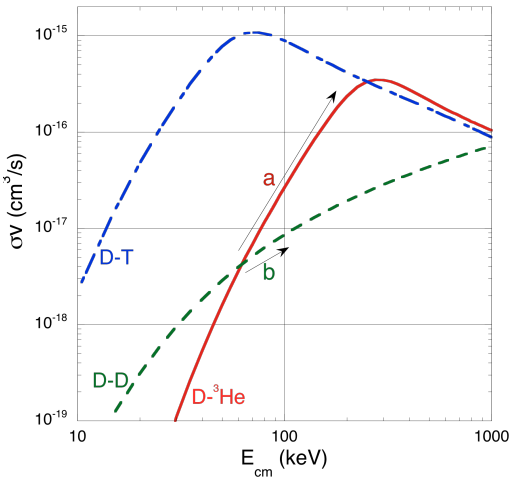

Figure 3. Fusion reaction rates vs center-of-mass energy, E_{cm}, for three sets of collision partners. At ion energies below 250 keV, the D–^{3}He fusion rate coefficient increases more rapidly with energy than does the D–D rate coefficient.

Add to this the larger surface-to-volume ratio ($\propto$ 1/radius) for a small (25 cm) FRC compared to a large (10 m) tokamak and an additional 40-fold reduction of neutron load on the wall is obtained. Overall, the shielding requirements for this type of small, clean reactor are far less, about a factor of ten in thickness, than for a D–T fueled larger fusion engine.

The RMF$_o$ method also offers the possibility of a novel direct energy-extraction method from the fusion products. The same rotating azimuthal electric field that accelerates keV ions up to several hundred keV can be used to extract energy from the fusion products, 3.6 MeV alphas and 14.7 MeV protons. Figure 4 shows minimum energy and the last energy of 4.2 MeV alpha particles as a function of the initial phase of the RMF after a 1 ms exposure to RMF$_o$. Depending on phase, a maximum of 2/3 of their energy was seen to be extracted in these single-particle Hamiltonian simulations. Including Coulomb scattering or RMF chirping is expected to increase the number of particles participating in this inverse Landau damping process. The reduction in particle energy is caused by an extraction of energy by the RMF$_o$ antenna. Thus, RMF$_o$ could provide both a high-efficiency way of extracting energy directly from the charged fusion products in addition to a way to maintain the center-of-mass ion energy for the D–^{3}He collision near the peak of its reactivity.

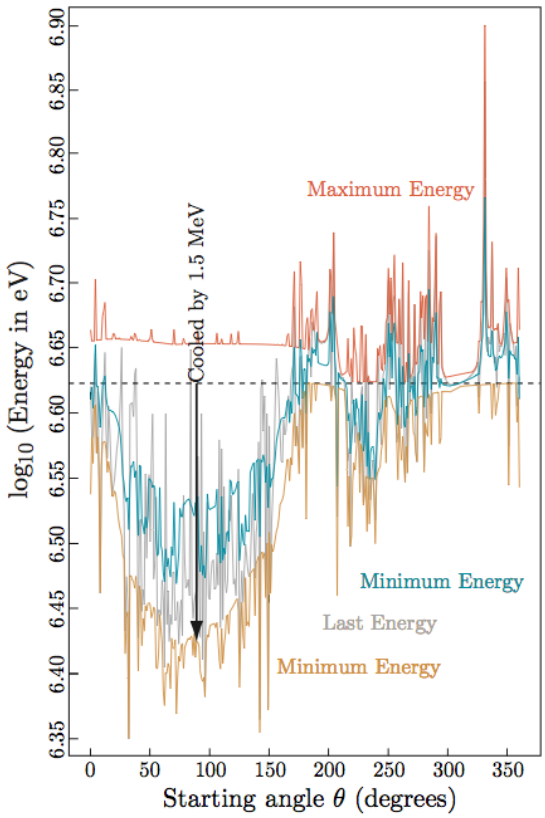

Figure 4. Minimum and last energy vs. RMF$_o$ initial phase for 4.5 MeV ^{4}He^{+2} in a 25 cm, 8 T FRC.

2.4 Status of RMF$_o$/FRC Development

No FRC has yet to achieve the parameters necessary for net power production by D–^{3}He fusion. A four step development plan has been proposed as laid out in Figure 6. Each PFRC device (Princeton Field Reversed Configuration, a designation used at PPPL) is listed with its significant milestone:

PFRC-1: Demonstrate electron heating by RMF$_o$

PFRC-2: Demonstrate ion heating to keV energies by RMF$_o$

PFRC-3: Demonstrate stable plasmas with 10 keV average particle energies

PFRC-4: Demonstrate net fusion production from steady state D–^{3}He RMF$_o$-heated plasma

To achieve these milestones, larger machines with stronger magnetic fields and higher heating power must be built.

PFRC-1 has accomplished its mission and PFRC-2 has been constructed (Figure 5); PFRC-2 has been constructed at Princeton Plasma Physics Laboratory (PPPL) with funds provided by the American Recovery and Reinvestment Act of 2009. PFRC-2 uses high-temperature superconductors for most of its confinement coils. The coils are cooled to liquid nitrogen temperatures and the currents are induced in the coils by the plasma. Hamiltonian scaling studies of PFRC-2, with a ten-fold increase in confining field and RMF power compared to its predecessor (PFRC-1), predicts the acceleration of ions to kilovolt energies given an existing equilibrium. First plasmas were made in October 2011. Tests of ion heating will begin in late 2012.

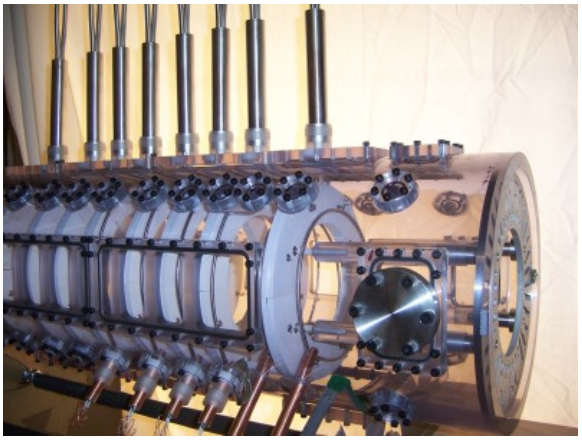

Figure 5. Princeton Plasma Physics Laboratory FRC vessel two (PFRC-2).

2.5 D–^{3}He Production

Helium-3 is needed for the fusion reaction. Helium-3 is scarce on the surface of the earth. In 2010 demand for ^{3}He was projected to be 76000 liters per year, but the United States only produces 8000 liters of ^{3}He a year. Moreover, last year the reported U.S. stockpile of ^{3}He was at less than 48000 liters [27]. ^{3}He currently costs $100 USD/liter. It is estimated that 26000 liters of ^{3}He could be produced per year as a byproduct of natural gas and helium production [28]. This would be a byproduct of helium production and would cost between $34 and $300 USD/liter. A plant to extract ^{3}He would cost several million dollars. The cost is based on extracting it from helium that is already produced. If ^{3}He were the sole product, the cost would be $12000 USD/liter. The atmosphere contains approximately 280 billion liters of ^{3}He but it is uneconomical to extract it from the air. Increased production of tritium, which decays to ^{3}He, in fission power plants is another option.

The mission discussed in this paper would require 10000–30000 liters of ^{3}He. This is in line with the amount that could be extracted in one year from U.S. natural gas sources. Even at $300/liter the fuel cost would be 1/10th the cost of an radioisotope thermal generator (RTG) and does not appear as an impediment to its use for spacecraft propulsion.

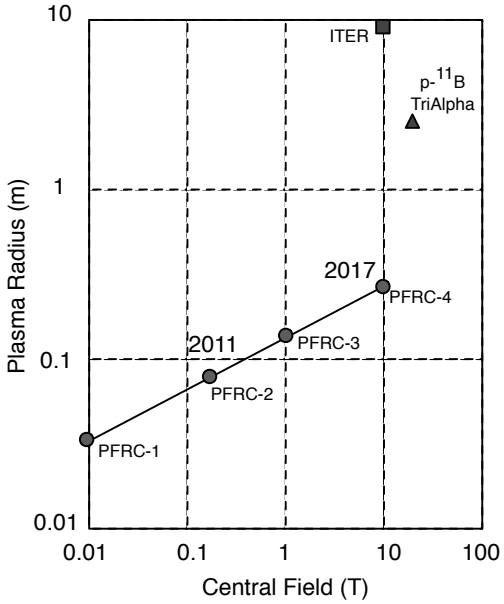

Figure 6. Fusion reactor development schedule. The plot also shows the size and field for the ITER tokamak, now under construction, and the proposed TriAlpha p–^{11}B FRC reactor. The plasma radius is defined as the distance from the major axis to plasma edge in the midplane. The central field for the tokamak is that on the magnetic axis while that for the FRC is on the midplane at the major axis.

2.6 Engine Design

2.6.1 Design The rocket engine we propose is shown schematically in Figure 1. It is roughly cylindrical in shape, about 6 m long and 1 m in diameter. The plasma containment vessel is ringed by coils that stabilize and confine the plasma, while RF antennas implement the RMF$_o$ heating scheme. Fusion occurs mainly in a hot plasma ellipsoid coaxial with the cylinder. The hot plasma is well confined within the ellipsoid. Outside of the ellipsoid is a region of cooler plasma which flows over the ellipsoid.

The primary design challenge for propulsion engineers is to efficiently convert the energy produced within the ellipsoid into usable thrust. As discussed in Section 2.1 energy from fusion reactions is carried initially in the kinetic energy of the fusion products. Most of these fusion products pass through the outer cooler plasma, predominantly heating electrons there. Also, a fraction of the fusion products' energy heats the electrons within the ellipsoid to temperatures near 50 keV. These hot electrons emit copious radiation, both as bremsstrahlung, mainly as X-rays, and as synchrotron radiation, with frequencies from 0.5 to 5 THz. The synchrotron radiation is efficiently absorbed by the cooler plasma shell. We estimate that the electron temperature in the shell will rise to near 300 eV.

The fusion products have a high velocity which makes them unsuitable for producing significant thrust. Thrust is increased by the addition of propellant, increasing mass flow and thrust [29]. In our design, cold gas is introduced at the "top" – the far left side – of the engine; see Figure 1. A suitable propellant would be deuterium injected at a rate of 150 mg/s. The gas would be ionized quickly, forming a plasma similar to what is called, in tokamak terminology, a high recycling divertor. The cold plasma will flow to the right, with electrons picking up energy from the fusion products and synchrotron radiation as it passes over the ellipsoid. The shell plasma thus formed and heated will be quite similar to that already produced in gas dynamic traps [30], having a density near 5×10^{13} cm^{-3} and an electron temperature of 100-300 eV. The ions will be cooler. As the plasma leaves the reactor, acceleration of the ions to an energy near $4T_e$ will occur in a double layer [31] near the nozzle throat. Within a few centimeters beyond the nozzle throat, the propellant will have acquired the desired 0.4–1.2 keV energy, (a velocity of 200 km/s), with a mass flow of 150 mg/s, sufficient to produce thrust of 30 N.

Table 3. JIMO mission Δu

Maneuver	Δu (km/s)
Earth departure	7.669
Callisto Orbit	3.184
Ganymede Orbit	3.621
Europa Orbit	2.567
Io Orbit	3.275
Jupiter Entry	8.204
Spiral Callisto to Ganymede	2.676
Spiral Ganymede to Europa	2.861
Spiral Europa to Io	3.591
Earth to Jupiter	93.63
Total	131.3

2.6.2 Radiation and Shielding Power will leave the plasma by four paths: charged particles, neutrons, bremsstrahlung, and synchrotron radiation. The energy in these channels might be lost without causing damage or they may damage the spacecraft structure. Alternatively, their energy may be captured and harnessed.

The reactor's neutron wall loading is 10^4 lower than a D–T tokamak of similar power output, which considerably reduces shielding requirements. Neutron shielding is necessary to protect the FRC's magnetic coils, RF antennae, and the electronics and structural components on-board the craft. The anticipated neutron fluence for this reactor over a mission lasting eighteen months to two years on the order of 10^{20} cm^{-2}. Extensive testing conducted for NASA's Project Prometheus, a proposed fission powered spacecraft, suggests that some combination of beryllium, boron carbide, lithium hydride, and tungsten would provide the best neutron shielding [32]. Following Rinard [33] and Miller [34], we find that, depending on the material composition and component, the shield thickness would range from 5–50 cm.

Shielding requirements can be reduced by locating the propellant tank of liquid D_2 between the reactor and the craft's body. The large neutron absorption cross section of D_2 could provide adequate protection even toward the end of the mission, when propellant levels have fallen. An insignificant amount of tritium, about one part in 10^{13}, would be produced by neutron capture. A thin layer of beryllium or tungsten between the reactor and the propellant tank would help to attenuate the neutron energies for better absorption. Further research is needed to determine the most suitable shielding material and layout for our specific application.

The bremsstrahlung, primarily in the form of X-rays, has an average energy of 50–100 kV and a total power output of 1.3 MW (Table 2). Less than 3 cm of X-ray shielding materials such as tungsten or lead would be required [35].

Synchrotron radiation produces the most power of the three types of radiation, on the order of 5–10 MW. Therefore, we not only want to consider shielding requirements but power absorption mechanisms as well. If the inner surface of the FRC chamber is smoothly polished then the synchrotron power will be reflected back into the plasma. By patterning the walls with reflective and non-reflective regions, the synchrotron radiation can be directed to rectennas and converted into power for the ship. An energy conversion efficiency of 1% would be sufficient to power the ship's sytems. Some of the reflected power will be absorbed by electrons on the outer edge of the ellipsoid and contribute to the heating of the cold plasma.

3. JUPITER ICY MOON ORBITER MISSION

3.1 Overview

To illustrate the capabilities of an aneutronic FRC fusion engine, we have analyzed the canceled Jupiter Icy Moon Orbiter Mission (JIMO). JIMO was to have a fission-based engine with ion thrusters. The time of flight to Jupiter was to be about six years. In our design the mission payload remains the same. The FRC-based engine has a power of 10 MW, and has its thrust enhanced from 100 mN to 30 N by propellant mass augmentation (see section 2.6.1). An orbital analysis has been done as described below, which indicates a time of transit between Earth and Jupiter of eighteen months.

The goals for the JIMO mission are

1. to determine the evolution and present state of the Galilean satellite surfaces and sub-surfaces, and the processes affecting them,

2. to determine the interior structures of the icy satellites in relation to the formation and history of the Jupiter system, and the potential "habitability" of the moons,

3. to search for signs of past and present life and characterize the habitability of the Jovian moons with emphasis on Europa, and
4. to determine how the components of the Jovian system operate and interact, leading to the diverse and possibly habitable environments of the icy moons.

The mission bus is identical to the JIMO bus.

3.2 Mission Plan

The spacecraft is placed in a 400 km low earth orbit. This permits testing of the vehicle before earth departure without too much concern over atmospheric drag. The spacecraft will fit within the shroud of an Atlas IV or SpaceX Falcon 9 launch vehicle. The vehicle then accelerates halfway to Jupiter and decelerates the rest of the way to the planet. It then spirals into the orbit of Callisto. It spirals down to an altitude of 400 km. After surveying Callisto it spirals out of orbit around Callisto and then spirals from Callisto's orbit to Ganymede repeating the process until it reaches its final orbit around Io.

The mission design, including engine parameters, is given in Table 3 and Table 4. The spacecraft takes eighteen months to reach Jupiter, which happens to be the same time the Discovery II took to reach Jupiter in the movie *2001: A Space Odyssey*.

Table 4. JIMO mission design

Parameter	Value
Specific power	1.0 kW/kg
Specific mass	0.02 kg/kg
Thrust	30 N
Power	5 MW
Dry mass	6200 kg
Payload mass	1060 kg
Propellent mass	5800 kg
Exhaust Velocity	200 km/s
Time to Jupiter	540 days
Time for Δu	460 days

3.3 Payload

The payload is identical to the JIMO bus. The auxiliary payload is a Europa lander. No additional instruments have been added for the Io orbit mission.

3.4 Spacecraft Design

The JIMO spacecraft is used as the baseline design. The ion engines are removed from the spacecraft and the fission reactor and radiators are removed. A radiation shield protects the payload. The fuel and propellant tanks are situated between the shield and the spacecraft providing additional payload radiation shielding.

4. CONCLUSIONS

We have presented the outline of a design for a fusion powered rocket engine based on the Field Reversed Configuration, using D$-^3$He reaction as an energy source. Additionally, we have shown the feasibility of a Jupiter mission that is a factor of three to four shorter in duration than NASA's JIMO mission. Many of the key physics principles involved have been separately demonstrated. There still remain a number of questions regarding the operation and stability of the reactor, and significantly, a reactor of the type described here has not yet demonstrated fusion burn.

This engine is even more attractive for longer missions where a lower thrust version of the engine, having a propellant mass ratio near unity, provides efficiencies that other engines cannot achieve.

ACKNOWLEDGMENTS

We thank Dr. T. Kornack for calculations on energy extraction by RMF$_o$. This work was supported, in part, by DOE contract No. DE-AC02-09CH11466.

Table 5. Payload

Instrument	Mass (kg)	Power (W)	Power Max (W)	Location
Super High-Res Camera (SHRC)	65	100	100	scan platform
High Res Telescope (NAC)	20	5	5	scan platform
Mapping Camera (MAC)	5	5	5	scan platform
Wide-angle Camera (WAC)	3	5	5	scan platform
Hyperspectral Imager (HSI)	25	15	15	scan platform
Thermal Imager (TI)	11	14	14	scan platform
SAR Topographic Mapper (TSAR)	150	200	1400	bus-mounted (on boom)
Ice Penetrating Radar (IPR)	50	2700	13000	bus-mounted
Laser-illumination Spectrometer (LIS)	250	2500	2500	bus-mounted
Laser Altimeter (LA)	44	1400	1400	bus-mounted
Plasma Wave Spectrometer (PWS)	10	7	7	bus-mounted
Magnetometer (MAG)	3	3	3	bus-mounted (on boom)
Ion and Neutral Mass Spectrometer (INMS)	10	28	28	Turntable
Heavy Ion Counter (HIC)	3.3	7	7	Turntable
Energetic Particle Detector (EPD)	11	10	10	Turntable
Plasma Spectrometer (PS-particles)	13	11	11	Turntable
Dust Detector (DD)	5	6	6	Turntable
Auxiliary Science Package (ASP)	375			bus-mounted
Total	1053	7000	18500	

REFERENCES

[1] Bramanti, C., Walker, R., Sutherland, O., Boswell, R., Charles, C., Frigot, P., Orlandi, M., del Amo, J., and Fearn, D., "The Innovative Dual-Stage 4-Grid Ion Thruster Concept–Theory And First Experimental Results," IAC-06-C4. 4.7 presented at 57th International Astronautical Congress, Valencia, Spain, 2006.

[2] Sawan, M., Zinkle, S., and Sheffield, J., "Impact of tritium removal and He-3 recycling on structure damage parameters in a D-D fusion system," *Fusion Engineering and Design*, Vol. 61-62, November 2002, pp. 561–567.

[3] Khvesyuk, V. I., Shabrov, N. V., and Lyakhov, A. N., "Ash Pumping From Mirror and Toroidal Magnetic Confinement Systems," *Fusion Technology*, Vol. 27, 1995, pp. 406–408.

[4] Romanellia, F., Brunob, C., and Regnolia, G., "Assessment of Open Magentic Fusion for Space Propulsion," Tech. Rep. 18853/05/NL/MV, The European Space Research and Technology Centre, 2005.

[5] Teller, E., Glass, A., Fowler, T. K., Hasegawa, A., and Santarius, J. F., "Space Propulsion by Fusion in a Magnetic Dipole," *Fusion Technology*, Vol. 22, 1992, pp. 82–97.

[6] Emrich Jr, W. J., "End Plugging in the Gasdynamic Mirror Using a Field Reversed Configuration," *Mini-Conference on Plasma Propulsion Physics: Fusion and High Energy Propulsion*, No. GM2.05, November 1999.

[7] Williams, C., Borowski, S., Dudzinski, L., and Juhasz, A., "A Spherical Torus Nuclear Fusion Reactor Space Propulsion Vehicle Concept for Fast Interplanetary Piloted and Robotic Missions," *Bulletin APS*, Vol. 4, No. 7, 1999, pp. 132.

[8] Williams, C., Borowski, S., Dudzinski, L., and Juhasz, A., "Realizing 2001: A Space Odyssey: Piloted Spherical Torus Nuclear Fusion Propulsion," Tech. Rep. NASA/TM?2005-213559, NASA Glenn Research Center, March 2005.

[9] Statham, G., White, S., Adams, R., Thio, Y., Alexander, R., Fincher, S. an Philips, A., and Polsgrove, T., "Engineering of the Magnetized Target Fusion Propulsion System," *AIAA*, No. 2003-4526, July 2003.

[10] Slough, J., "Performance Capability and Mission Analysis for a Pulsed High Density FRC Fusion Rocket," *AIAA*, No. 2001-3674, AIAA, July 2001.

[11] Gorelenkov, N., Zakharov, L., Bhatta, P., and Paluszek, M., "Magnetic Fusion Engine," *43rd AIAA/ASME/SAE/ASEE Joint Propulsion Conference and Exhibit*, AIAA/ASME/SAE/ASEE, 2007.

[12] Cheung, A., Binderbauer, M., Liu, F. Qerushi, A., Rostoker, N., and Wessel, F. J., "Colliding Beam Fusion Reactor Space Propulsion System," *Space Tehcnologies and Applications International Forum*, No. CP699, 2004.

[13] Lampe, M. and Manheimer, W., "Comments on the Colliding Beam Fusion Reactor Porposed by Rostoker, Binderbauer, and Monkhorst for use with the p-11B Fusion Reaction," Tech. Rep. NRL/MR/6709–98-8305, Naval Research Laboratory, October 1998.

[14] Miller, K., Slough, J., and Hoffman, A., "An Overview of the Star Thrust Experiment," *Space technology and applications international forum*, Vol. 420, AIP Conference Proceedings, http://depts.washington.edu/rppl/programs/stx.pdf, 1998, pp. 1352–1358.

[15] Tuszewski, M. A., "Field Reversed Configurations," *Nuclear Fusion*, Vol. 28, No. 11, November 1988, pp. 2033.

[16] Blevin, H. and Thonemann, P., *Nuclear Fusion Supplement*, Vol. 1, 1962, pp. 55.

[17] Binderbauer, M., Guo, H. Y., M.Tuszewski, Putvinski, S., Sevier, L., and Barnes, D., "Dynamic Formation of a Hot Field Reversed Configuration with Improved Confinement by Supersonic Merging of Two Colliding High-Compact Toroids," *Physical Review Letters*, Vol. 105, 2010, pp. 045003.

[18] Wesson, J., *Tokamaks*, Oxford Univ. Press, Oxford, 3rd ed., 2004.

[19] Cohen, S. A., Berlinger, B., Brunkhorst, C., Brooks, A., Ferarro, N., Lundberg, D., Roach, A., and Glasser, A., "Formation of Collisionless High- Plasmas by Odd-Parity Rotating Magnetic Fields," *Physical Review Letters*, Vol. 98, 2007, pp. 145002.

[20] Rosenbluth, M. N. and Bussac, M. N., "MHD Stability of Spheromak," *Nuclear Fusion*, Vol. 19, 1978, pp. 489.

[21] Glasser, A. and Cohen, S. A., "Ion and electron acceleration in the Field-reversed configuration with an odd-parity rotating magnetic field," *Physics of Plasmas*, 2002, pp. 2093–2102.

[22] Landsman, A. S., Cohen, S. A., and Glasser, A., "Onset and saturation of ion heating by odd-parity rotating magnetic fields in an FRC," *Physical Review Letters*, Vol. 96, 2006, pp. 015002.

[23] Cohen, S. A., Landsman, A. S., and Glasser, A., "Stochastic ion heating in a field-reversed configuration geometry by rotating magnetic fields," *Physics of Plasmas*, Vol. 14, 2007, pp. 072508.

[24] Cohen, S. A., Berlinger, B., Brooks, A., Brunkhorst, C., Glasser, A., Ferarro, N., Landsman, A., Lundberg, D., and Roach, A., "RMF0-Formed Collisionless High- Plasmas: Yesterday, Today, and Tomorrow," Tech. Rep. DE-AC02-76-CHO-3073, Princeton Plasma Physics Laboratory, DOE, 2007.

[25] Rider, T., "Fundamental limitations on plasma fusion systems not in thermodynamic equilibrium," *Physics of Plasmas*, Vol. 4, 1997, pp. 1039.

[26] Welch, D., Cohen, S. A., Genoni, T. C., and Glasser, A., "Formation of field-reversed-configuration plasmas with punctuated-betatron-orbit electrons," *Physical Review Letters*, Vol. 105, 2010, pp. 015002.

[27] "Helium-3 Shortage Endangers Nuclear Detection Capabilities," `http://www.homelandsecuritynewswire.com/helium-3-shortage-endangers-nuclear-detection-capabilities`, February 2011, accessed 25 April 2012.

[28] Shea, D. and Morgan, D., "The Helium-3 Shortage: Supply, Demand, and Options for Congress," Tech. Rep. 7-5700 R41419, Congressional Research Service, www.crs.gov, December 2010.

[29] Santarius, J. F., "Lunar He-3, fusion propulsion, and space development," *Lunar Bases and Space Activities of the 21st Century*, edited by W. W. Mendell, J. W. Alred, L. S. Bell, M. J. Cintala, T. M. Crabb, R. H. Durrett, B. R. Finney, H. A. Franklin, J. R. French, & J. S. Greenberg, Sept. 1992, pp. 75–81.

[30] Anikeev, A., Bagryansky, P., Ivanov, A., Karpushov, A., Noack, K., and Strogalova, S., "Upgrade of The Gas Dynamic Trap: Physical Concepts and Numerical Models," *28th EPS Conference on Controlled Fusion and Plasma Physics, Funchal*, Vol. ECA, 25A, 2001, p. 121.

[31] Cohen, S., Siefert, N., Stange, S., Boivin, R., Scime, E., and Levinton, F., "Ion acceleration in plasmas emerging from a helicon-heated magnetic-mirror device," *Physics of Plasmas*, Vol. 10, 2003, pp. 2593.

[32] Lewis, R., "Space Shielding Materials for Prometheus Application," Tech. Rep. MDO-723-0049, Knolls Atomic Power Laboratory, January 2006.

[33] Rinard, P., *Passive Nondestructive Assay of Nuclear Materials*, chap. 12: Neutron Interactions with Matter, Nuclear Regulatory Commission, 1991, p. 364.

[34] Miller, D., Adair, R., Bockelman, C. K., and Darden, S. E., "Total Cross Sections of Heavy Nuclei for Fast Neutrons," *Physical Review*, Vol. 88, No. 1, October 1952, pp. 83–90.

[35] Gerward, L., Guilbert, N., Jensen, K., and Levring, H., "WinXCom—a program for calculating X-ray attenuation coefficients," *Radiation Physics and Chemistry*, Vol. 71, No. 3, 2004, pp. 653–654.